Electronic Supplementary Material (ESI) for Journal of Materials Chemistry C.

Electronic Supplementary Material

Synthesis of Tuneable Au Nanostars: the Role of Adenosine Monophosphate

Carlos Fernández-Lodeiro,[1,2] Javier Fernández-Lodeiro, (✉)[3,4] Adrián Fernández-Lodeiro, [3,4] Silvia Nuti, [3,4] Carlos Lodeiro, [3,4] Alec Lagrowth,[5] Ignacio Pérez-Juste,[2] Jorge Pérez-Juste(✉)[1,2] and Isabel Pastoriza-Santos(✉)[1,2]

[1]CINBIO, Universidade de Vigo, Campus Universitario As Lagoas, Marcosende, 36310 Vigo, Spain.
[2]*Departamento de Química Física, Universidade de Vigo, Campus Universitario As Lagoas, Marcosende, 36310 Vigo, Spain.*
[3]*BIOSCOPE Group, LAQV@REQUIMTE, Chemistry Department, Faculty of Science and Technology, University NOVA of Lisbon, Caparica Campus, 2829-516 Caparica, Portugal*
[4]*PROTEOMASS Scientific Society, Rua dos Inventores, Madam Parque, Caparica Campus, 2829-516 Caparica, Portugal*
[5]*International Iberian Nanotechnology Laboratory, Braga, 4715-330, Portugal*

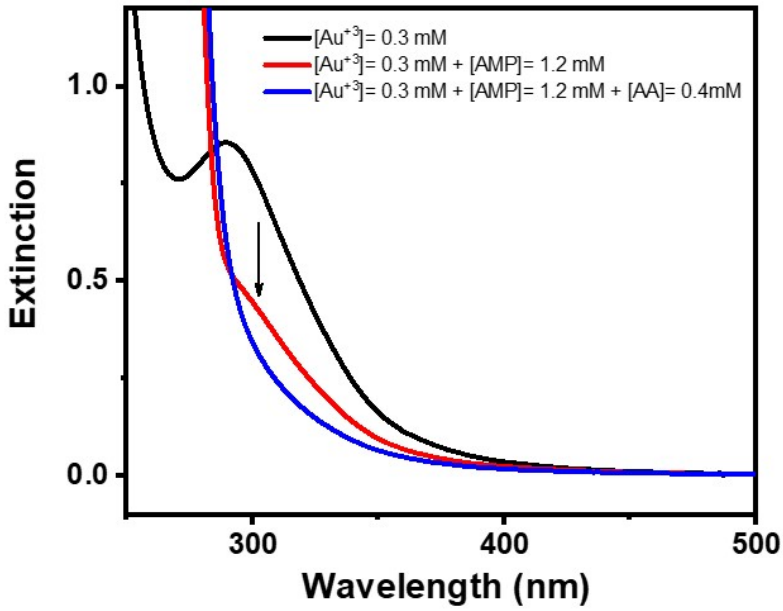

Figure S1. Spectrophotometric study of $HAuCl_4$ reduction with AA in the presence of AMP ([$HAuCl_4$] = 0.3 mM, [AA] = 0.4 mM, [AMP] = 1.2 mM). The arrow indicates the Au(III) CTT that disappears upon the addition of ascorbic acid.

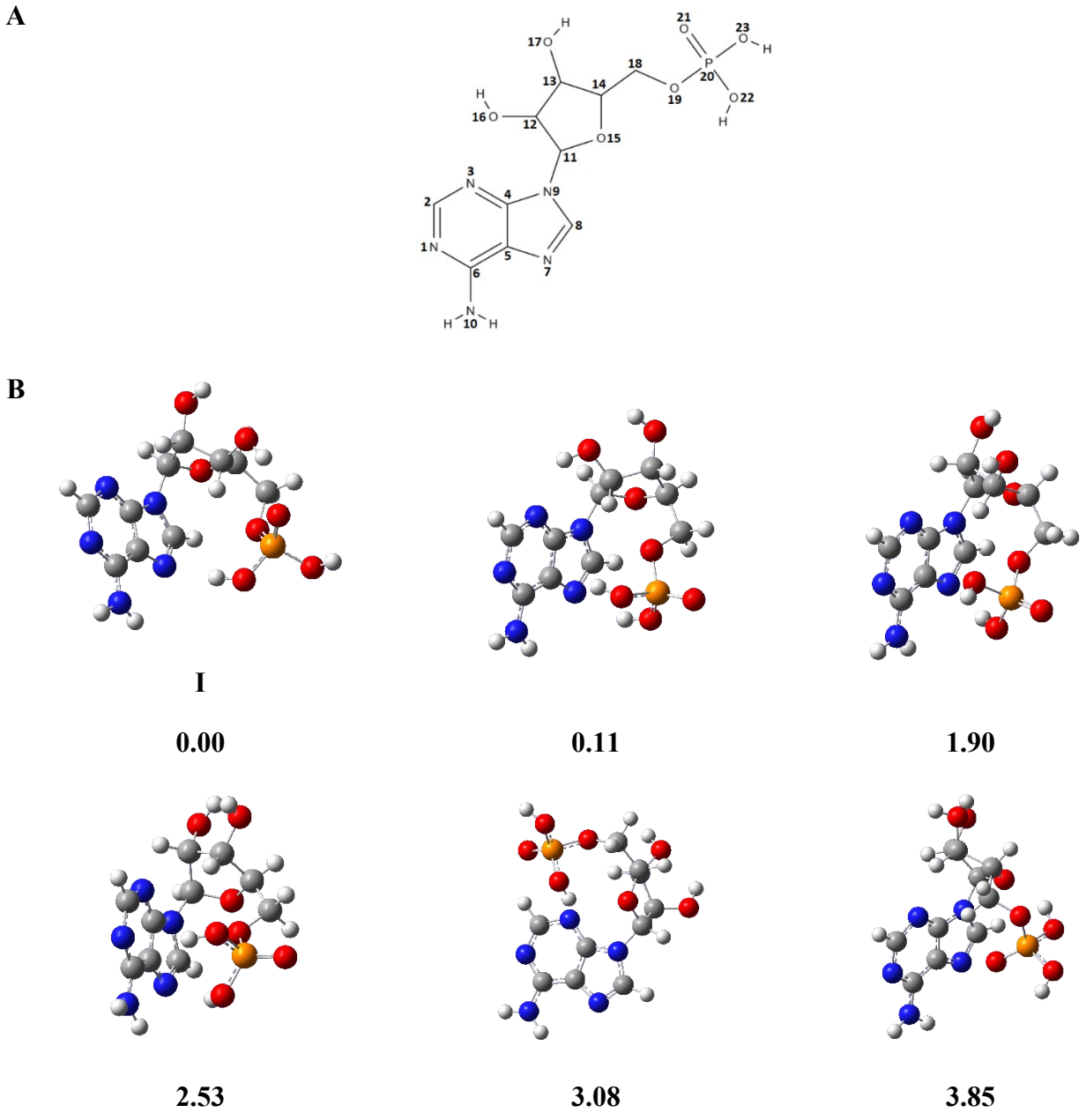

Figure S2. Conformational analysis of AMP. (A) Atom numbering employed for AMP. (B) AMP gas phase stable conformers and their relative energies computed at the M062X/6-311+G* level (values between brackets in kcal/mol).

As starting point for the theoretical study, we performed a preliminary gas phase conformational analysis of AMP employing the GMMX method and DFT calculations. The results obtained (Figure S2) predict several stable conformers for AMP within an energy interval of 10 kcal/mol. The most stable conformer, labeled as **I**, shows a geometrical disposition with the six-membered ring of the adenine unit in *anti* orientation with respect to the ribose ring and the phosphate group bent over the

adenine ring. This structure, strongly stabilized by the presence of two intermolecular hydrogen bonding between one of the P=O and one of the ribose O-H units and between one of the PO-H bonds and the N7 atoms of the adenine ring, has been taken as the starting point for the forthcoming calculations on the complexation of AMP with the $AuCl_4^-$ salt.

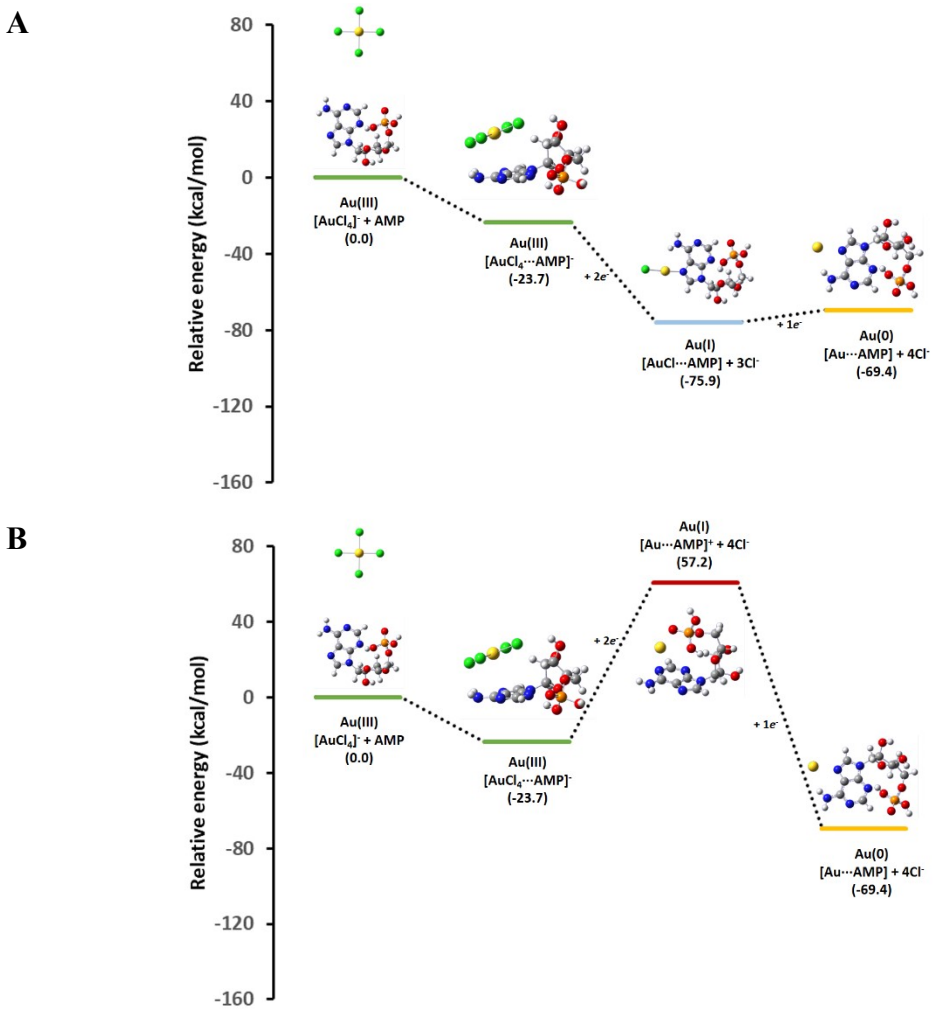

Figure S3. AMP complexation with $AuCl_4^-$. Theoretical energy profiles proposed for the interaction of $AuCl_4^-$ with AMP and the Au(III)®Au(0) reduction: In the presence of ascorbic acid, the $[AuCl_4\cdots AMP]^-$ complex formed by the initial interaction between the reactants can reduce to different **(A)** [AuCl···AMP], or **(B)** $[Au\cdots AMP]^+$ species. In all cases, the reduction to [Au···AMP] species is not favorable, which suggested that the addition of Au(0) seeds is needed.

Interestingly, theoretical explorations of different complexation mechanisms predict always less favoured energy paths than the one shown in Figure 1 in the main text. This is the case if the first stage of the interaction between $AuCl_4^-$ and AMP takes place through the formation of an Au-N bond, which suggests that the energy required for breaking one of the Au-Cl bonds in $AuCl_4^-$ is larger than the energy stabilization due to the formation of a new bond Au-N bond (Figure S3). Even more, it must be also noted that our calculations indicate that the most favorable energy path for the reduction of the initial $[AuCl_4\cdots AMP]^-$ complex is the one accompanied by the release of two chloride atoms, while those paths where three or four chloride atoms are released upon reduction are less favored energetically and, as a consequence, the presence of other reduced Au(I) species as [AuCl···AMP] and $[Au\cdots AMP]^+$ are expected to be less probable (see also Figures S3 and S4).

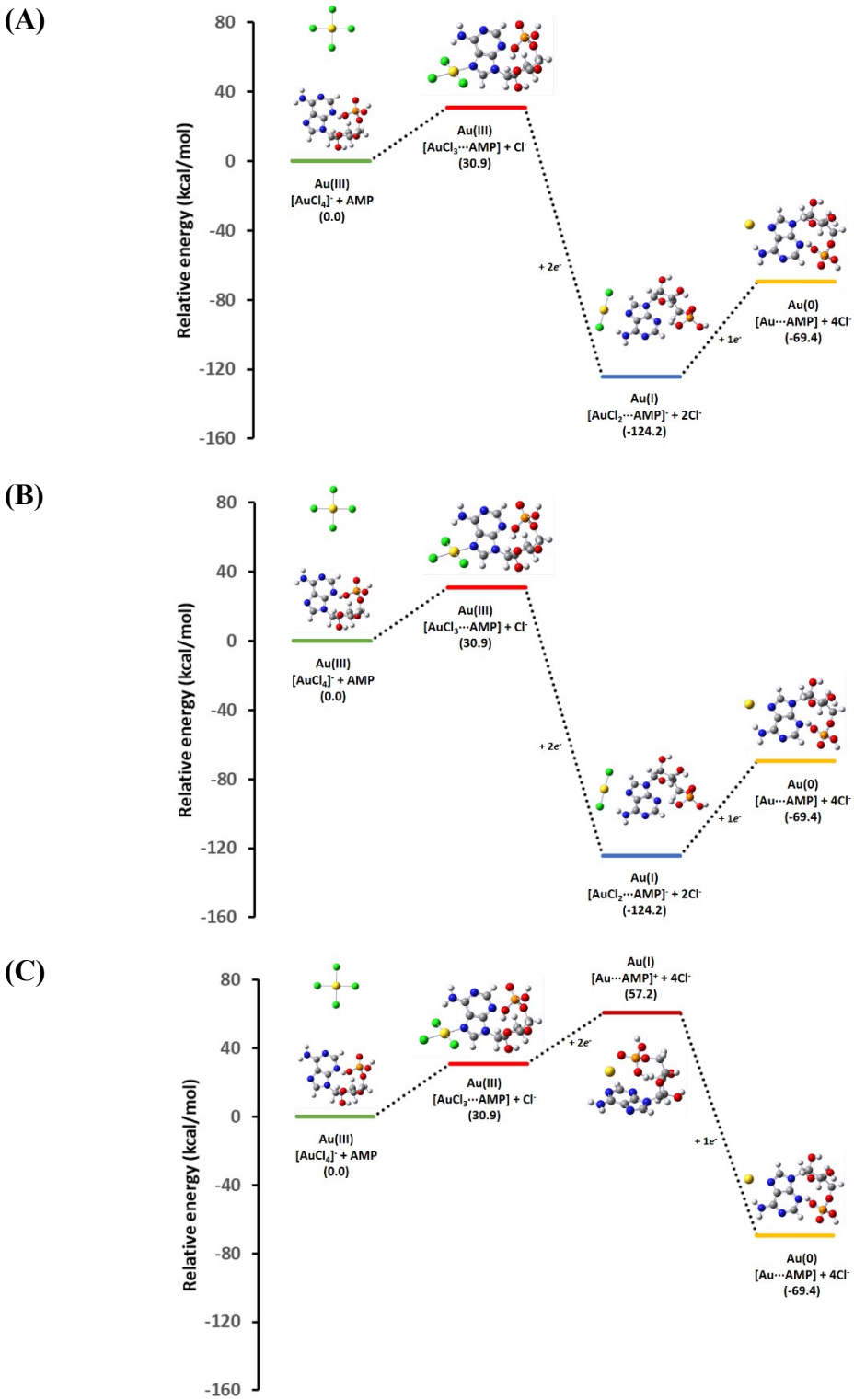

Figure S4. AMP complexation with $AuCl_4^-$. Theoretical energy profiles proposed for the interaction of $AuCl_4^-$ with AMP and the Au(III)/Au(0) reduction: In the presence of ascorbic acid, the [$AuCl_3$···AMP] complex formed by the initial interaction between the reactants can reduce to different **(A)** [$AuCl_2$···AMP]$^-$, **(B)** [AuCl···AMP], or **(C)** [Au···AMP]$^+$ species. Additional reduction of these latter forms in the presence of Au seeds would produce the [Au···AMP] complex.

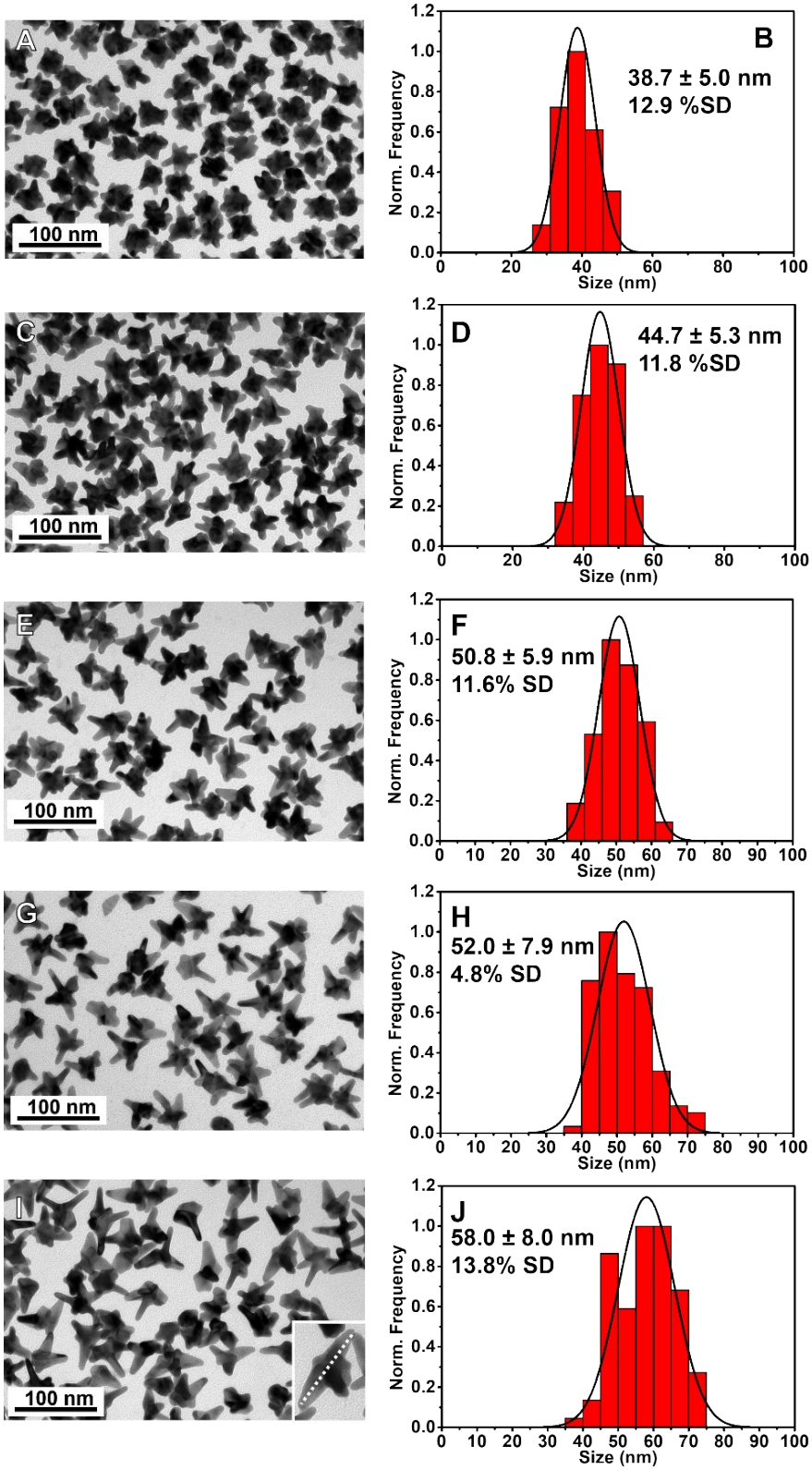

Figure S5. Representative TEM images of Au NSs synthesized with different AMP concentration (left) and their corresponding size distribution histograms (right). (A, B) 0.5 mM AMP, (C, D) 0.6 mM AMP, (E, F) 0.7

mM AMP, (G, H) 0.8 mM AMP and (I, J) 0.9 mM AMP. The inset in I represents how the NPs were measured.

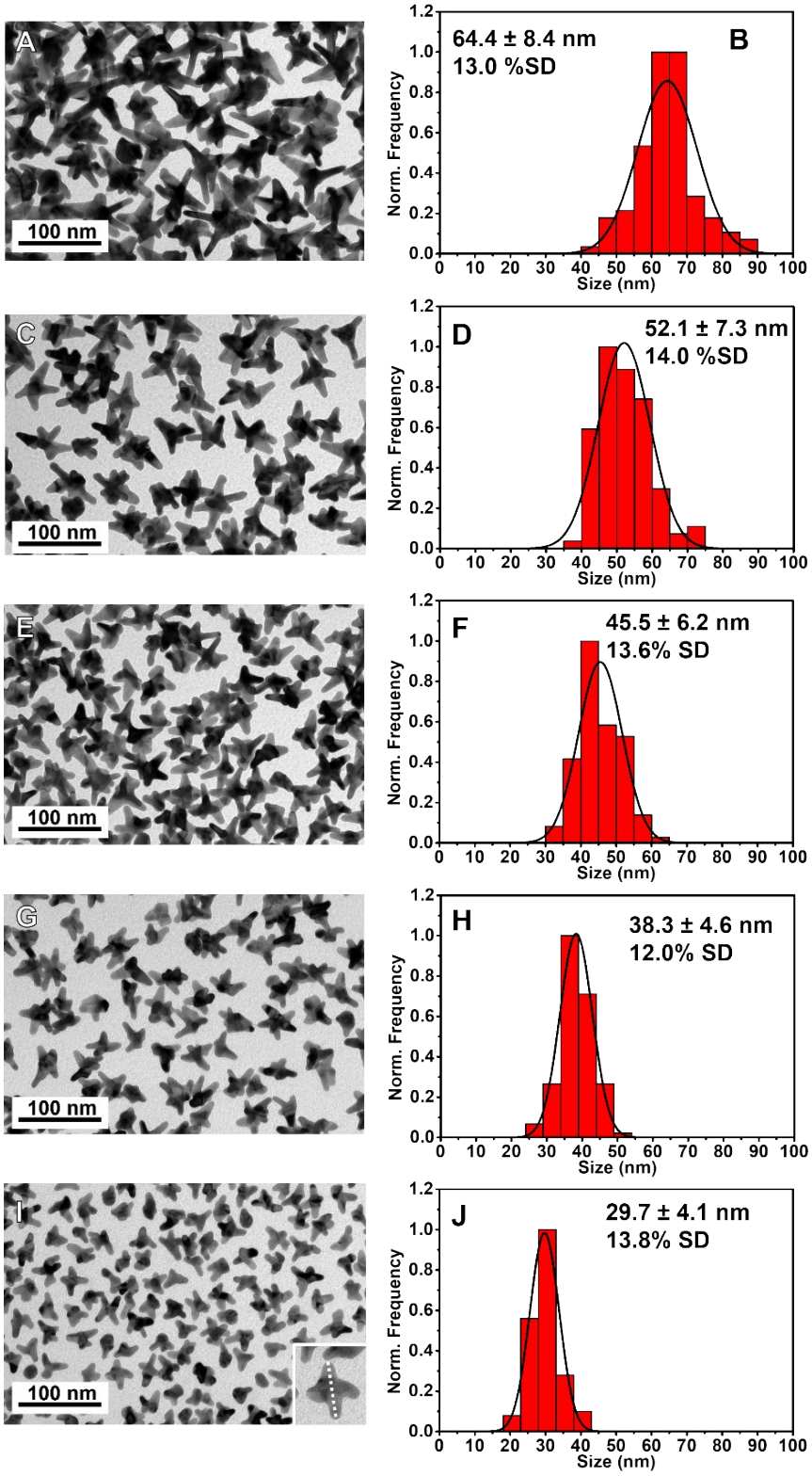

Figure S6. Representative TEM images of Au NSs synthesized with different seeds concentration (left) and their corresponding size distribution histograms (right). (A,B) 160 pM of seeds, (C,D) 320 pM of seeds, (E,F) 480 pM of seeds, (G,H) 640 pM of seeds and (I,J) 1200 pM of seeds. The inset in I represents how the NPs were measured.

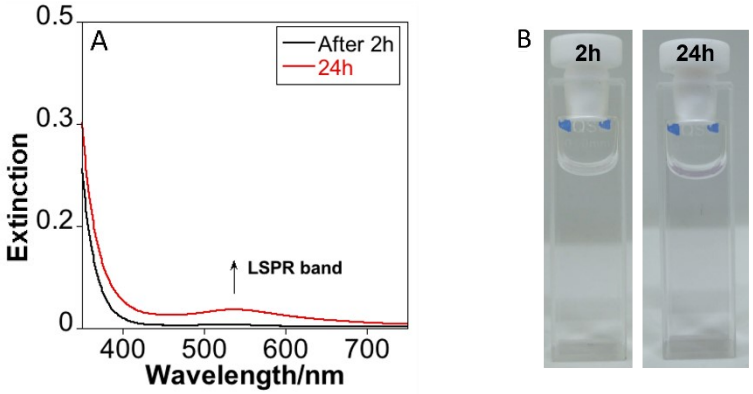

Figure S7. (A) UV-Vis extinction spectra of the $HAuCl_4$ reduction with ascorbic acid in the presence of AMP and in the absence of Au seeds. [$HAuCl_4$] = 0.3 mM, [AA] = 0.4 mM, [AMP] = 1.2 mM. (B) Photographs of the solutions after 2 and 24 hours, as indicated, revealing a marginal Au reduction.

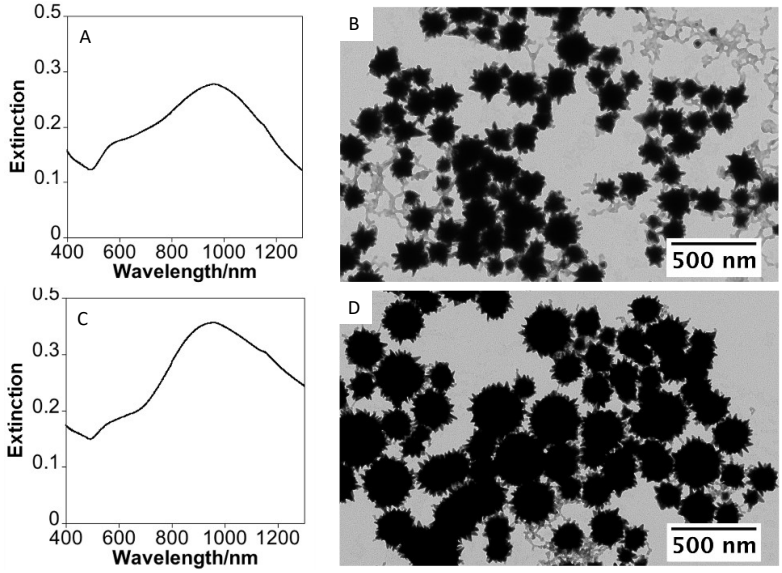

Figure S8. UV-Vis extinction spectra and representative TEM images after 24 hours of the $HAuCl_4$ reduction with ascorbic acid in the absence of Au seeds and in the presence of different AMP concentrations; 0.6 mM (A and B) and 0.3 mM (C and D). Constant parameters; [$HAuCl_4$] = 0.3 mM and [AA] = 0.4 mM.

If the AMP concentration is decreased to 0.6-0.3 mM, the formation of NPs becomes more favourable observing the formation of nonuniform star-shaped nanoparticles with sizes ranging between 50 to 300 nm after 24 h reaction (Figure S2) which exhibited a broad LSPR band at ca. 960 nm (see Figure S8). It should be also noted that under these conditions the reduction is not complete (only 20%).

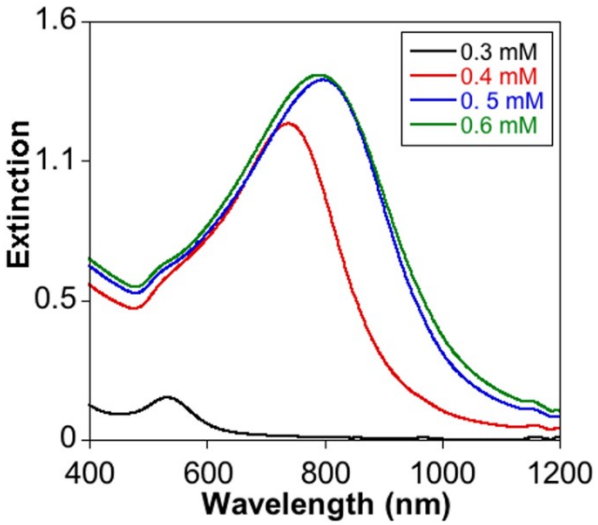

Figure S9. Extinction spectra of AuNSs synthesized using different ascorbic acid concentrations, as indicated. $[Au]_{seed}$= 320 pM, $[AuCl_4^-]$=0.3 mM and [AMP]= 0.7 mM at 40 ºC, kept constant in all cases.

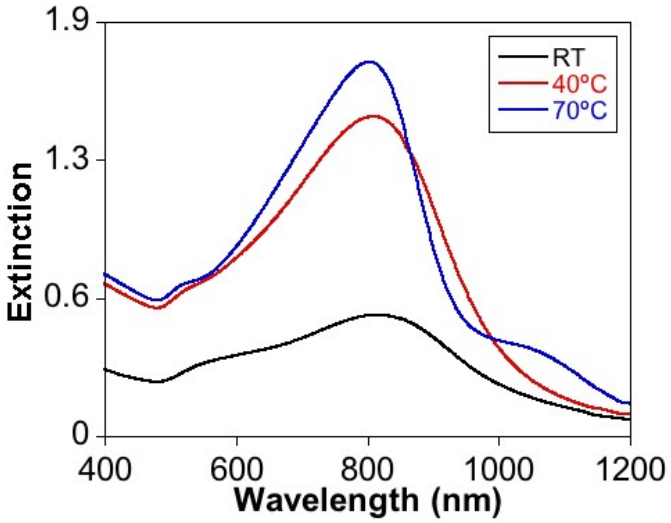

Figure S10. Extinction spectra of AuNSs synthesized under different temperatures, as indicated. $[Au]_{seed}$= 320 pM, $[AuCl_4^-]$=0.3 mM, [AA]= 0.5 mM and [AMP]= 0.7 mM, kept constant in all cases.

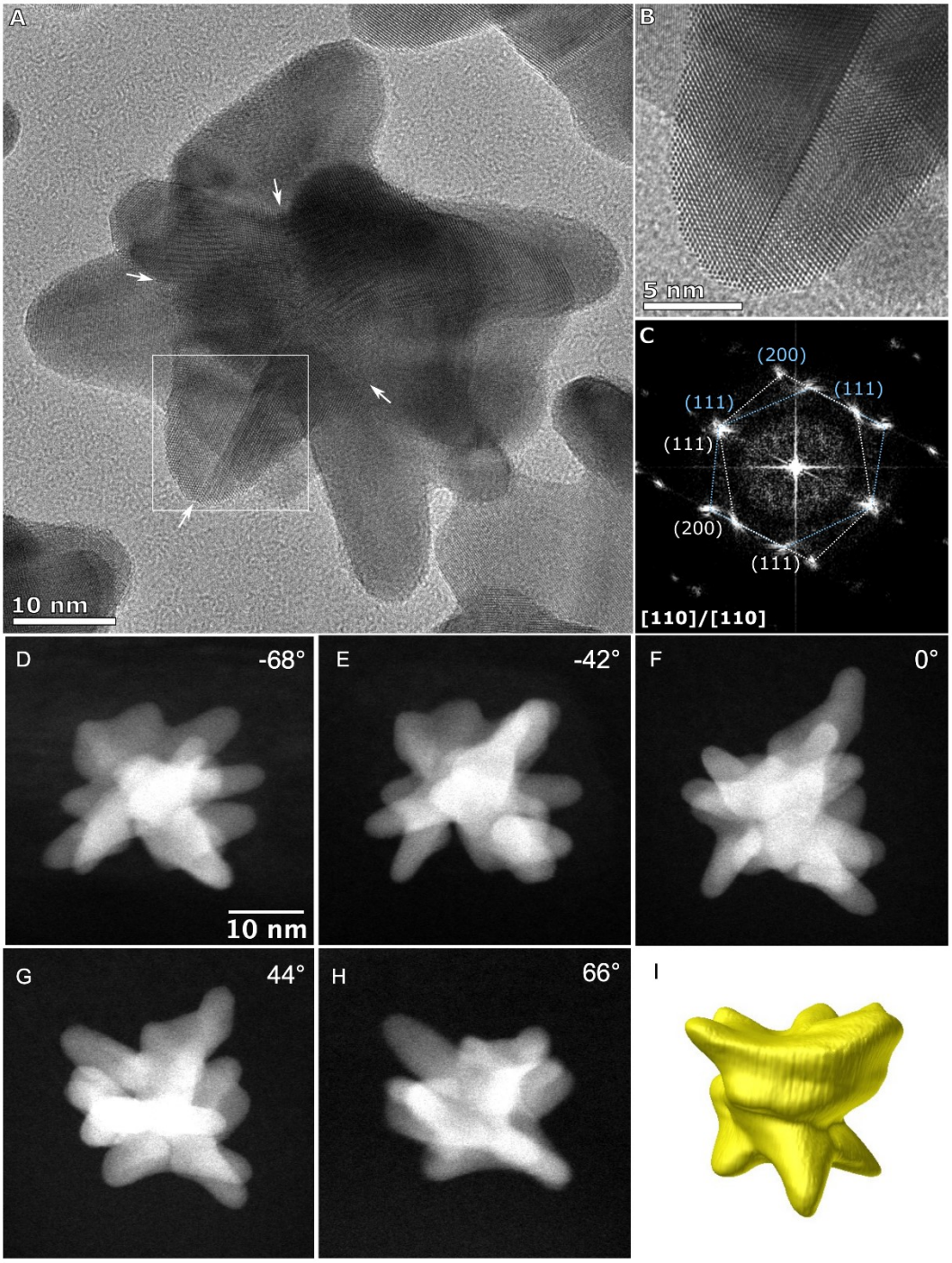

Figure S11. (A) Aberration corrected HR-TEM of a gold nanostar synthesized using 0.6 mM of AMP and 320 pM of seeds, the white arrows point towards twins in the arms. (B) Zoomed image of the branch taken from the white box in (A) with a defect plane running down the centre of the arm. The FFT taken from (B) is shown in (C) with two zone axes both viewed down the [110] axis twinned along the (111) spacing. (D-H) are the HAADF-STEM images taken from the tomography tilt series with the white arrows indicating when the defect plane can be clearly seen along the branches arm. (I) Reconstruction and 3D visualization of the tilt series.

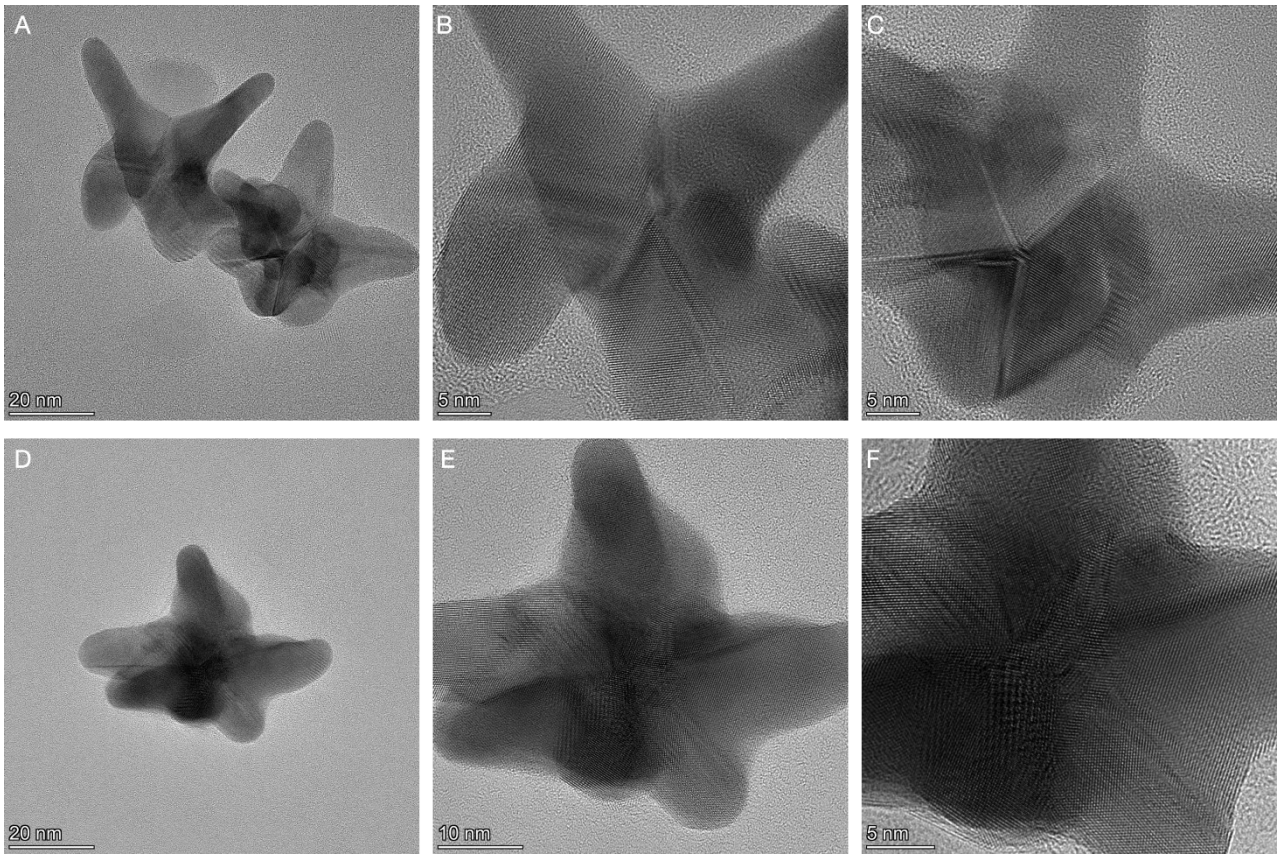

Figure S12. HR-TEM images of Au nanostars obtained using 0.9 mM (A-C) and 0.7 mM (D-F) of AMP showing the multi twinned crystallographic structure at the center of the nanoparticle.

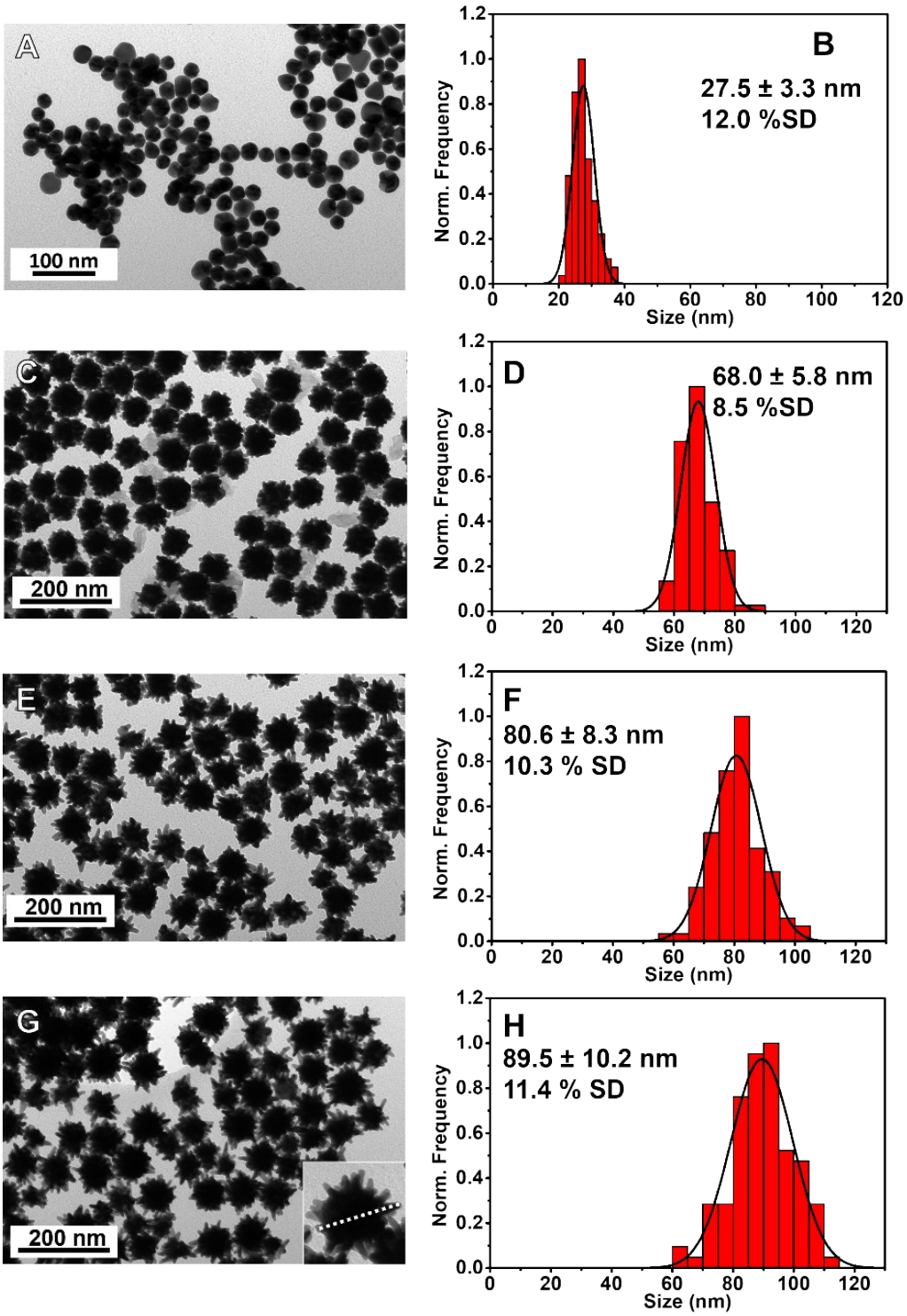

Figure S13. Representative TEM images of Au NSs synthesized with different AMP concentration (left) and their corresponding size distribution histograms (right). (A, B) 0.4 mM AMP, (C, D) 0.7 mM AMP, (E, F) 0.9 mM AMP. The inset in I represents how the NPs were measured.

Analysis of the effect of adsorption on the AMP conformational flexibility

The different conformations of AMP can be described by the O15-C11-N9-C4 dihedral angle (see Figure S2 for numbering): For values between 0±90º, the AMP conformation is denoted as *syn* (the six-membered adenine ring confronts the ribose ring), while for values between 180±90º, the conformation is characterized as *anti*.[1] On the other hand, the conformations of the ribose unit can be described by means of the C14-O15-C11-C12 (p_1) and C13-C14-O15-C11 (p_2) dihedral angles that define the puckering of the ribose ring: Structures with $p_1 > 0$ and $p_2 > 0$ correspond to C12 *exo* conformations and $p_1 < 0$ and $p_2 < 0$ correspond to C12 *endo* conformations, while $p_1 > 0$ and $p_2 < 0$ characterize O15 *exo* conformations and $p_1 < 0$ and $p_2 > 0$ identify O15 *endo* conformations.[2] According to the results depicted in Figure S10, MD simulations for isolated AMP in water show that the adenine ring adopts *syn* and *anti* orientations with respect to the ribose unit due to rotation around the central C-N bond between both rings, although the latter conformations are more frequent. In the same manner, the ribose group in free AMP adopt mostly O15 *endo* conformations ($p_1 < 0$ and $p_2 > 0$), although C12 *endo* conformations ($p_1 < 0$ and $p_2 < 0$) can also be found during the simulations (see Figure S11).

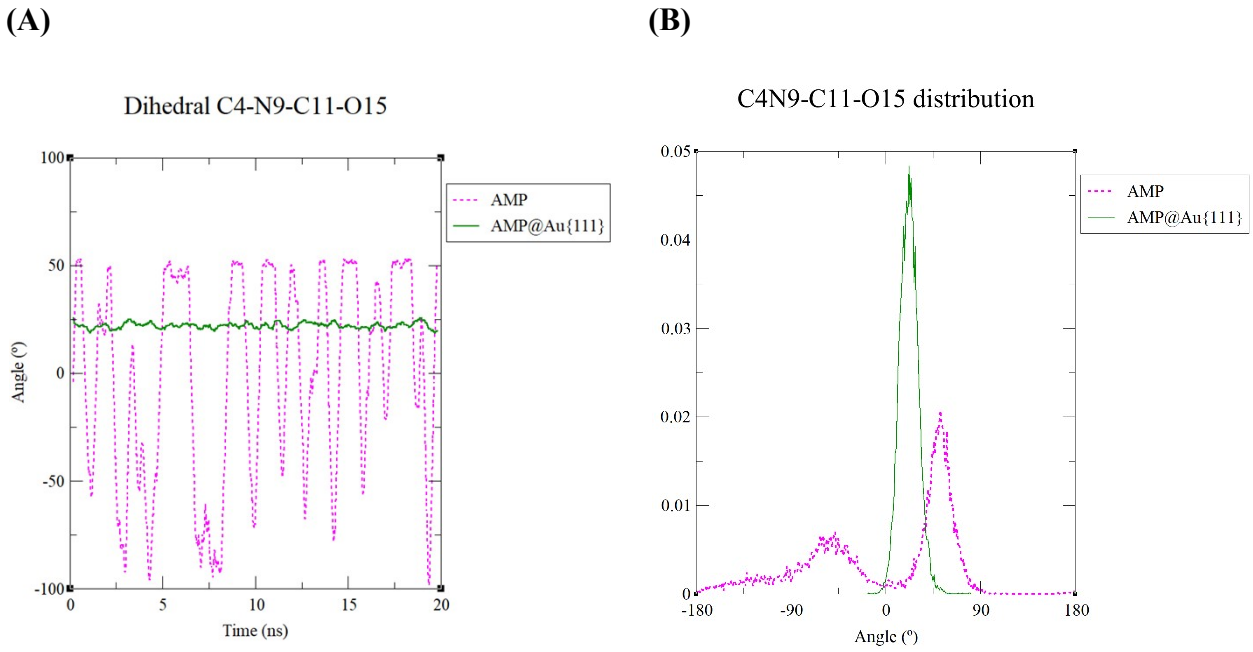

Figure S14. Relative orientation of the adenine and ribose units in isolated AMP (magenta line) and AMP adsorbed on the Au{111} slab (green line): Variation of the C4-N9-C11-O15 dihedral with time (A) and values distribution (B).

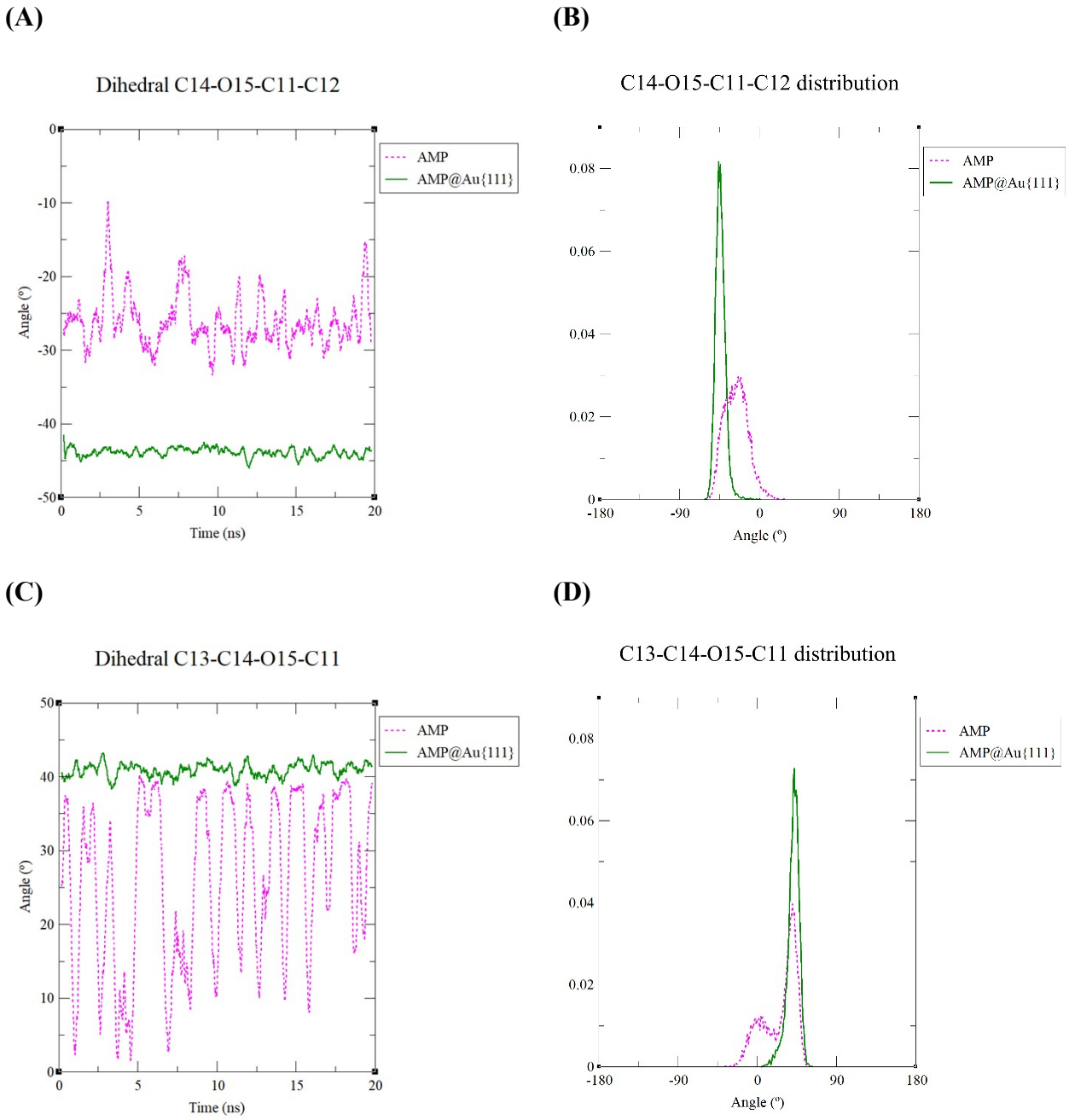

Figure S15. Characterization of the ribose unit in isolated AMP (magenta line) and AMP adsorbed on the Au{111} slab (green line): Puckering dihedrals C14-O15-C11-C12 and C13-C14-O15-C11 with time (A, C) and values distribution (B, D).

Interestingly, adsorption causes a considerable reduction of the AMP conformational flexibility compared to its behaviour in aqueous solution. On the one hand, the adenine and ribose rings only adopt *syn* dispositions and the average O15-C11-N9-C4 dihedral reduces until 22.0º. On the other hand, the strong interactions between the metal surface and the ribose oxygen restrain severely the puckering of the ring, so that the and the p_1 and p_2 dihedrals takes values oscillating slightly around their average values of -43.8º and 40.9º, respectively. Finally, the restrained mobility also extends to the phosphate group which rotates considerably around the P-C bond in isolated AMP in water, but remains almost fixed upon adsorption and showing dihedrals around 100º as a consequence of the direct interactions between the oxygen atoms of the phosphate group and the gold atoms on the surface (see Figure S12). It is Interesting to recall here that restrictions to conformational flexibility has been also found in ATP when comparing its behaviour in solution and interacting with proteins which can be related to protein activity.[2]

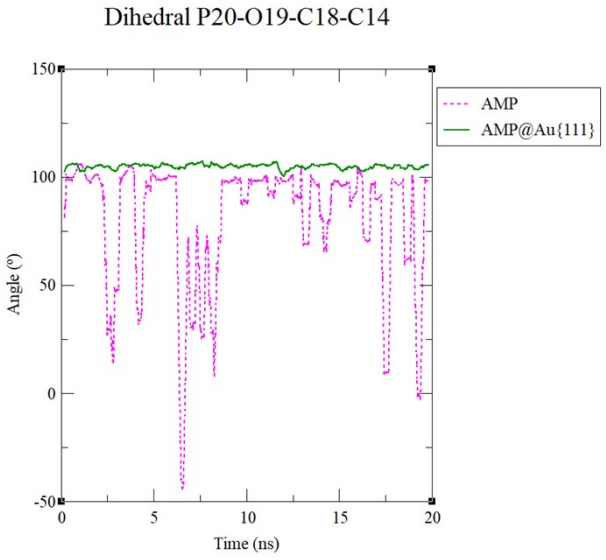

Figure S16. Rotation of the phosphate group in isolated AMP (magenta line) and AMP adsorbed on the Au{111} slab (green line): Variation of the P20-O19-C18-C14 dihedral with time.

(A) **(B)**

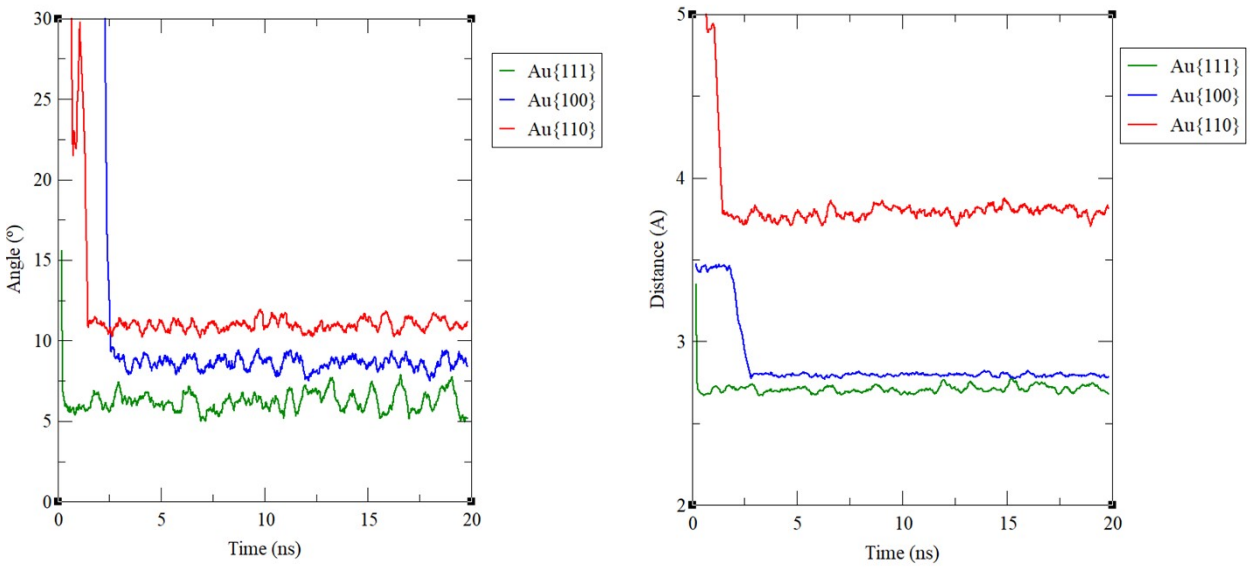

Figure S17. (A) Average angle between the adenine ring of AMP and the metal surface of the three gold slabs considered in this paper. (B) Average distance between the oxygen atom of the ribose ring and the metal surface of the {111}, {110} and {100} gold slabs.

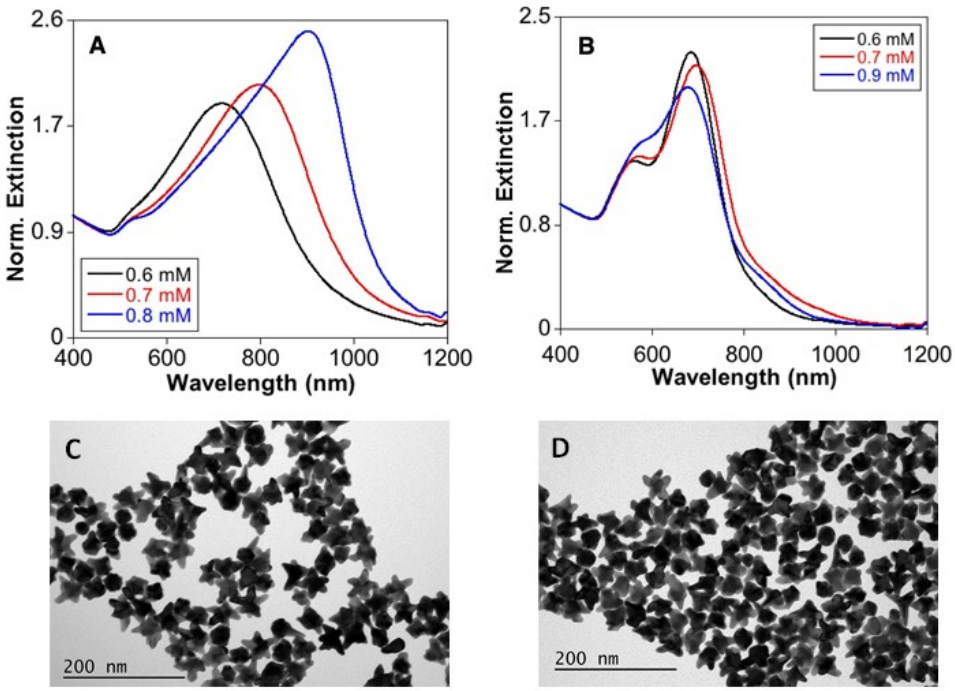

Figure S18. (A-B) Normalized extinction spectra of AuNSs obtained using different AMP (A) and GMP (B) concentration, as indicated. (C and D) Representative TEM images of AuNSs synthesized in the presence of GMP with a concentration of 0.6 mM (C) and 0.9 mM (D). [Au]seed= 320 pM, [$AuCl_4^-$]=0.3 mM and [AA]=0.5 mM.

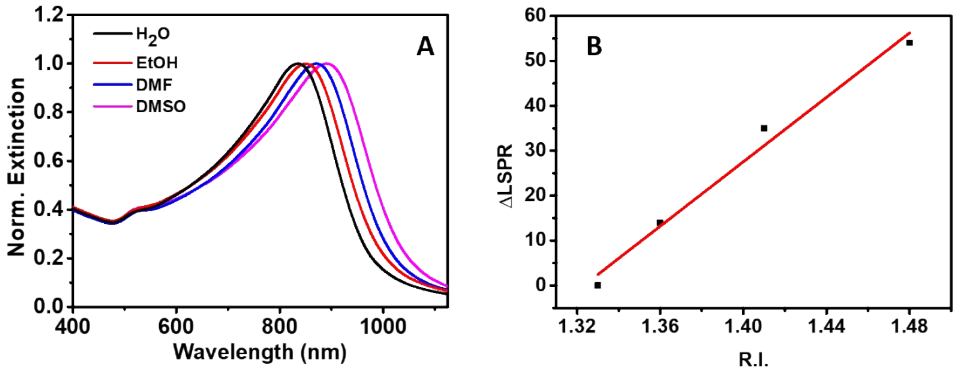

Figure S19. (A) Normalized extinction spectra of AMP-stabilized AuNSs redispersed in different solvents as indicated. (B) LSPR shift versus the refractive index for AuNSs with LSPR centered at 830 nm in water.

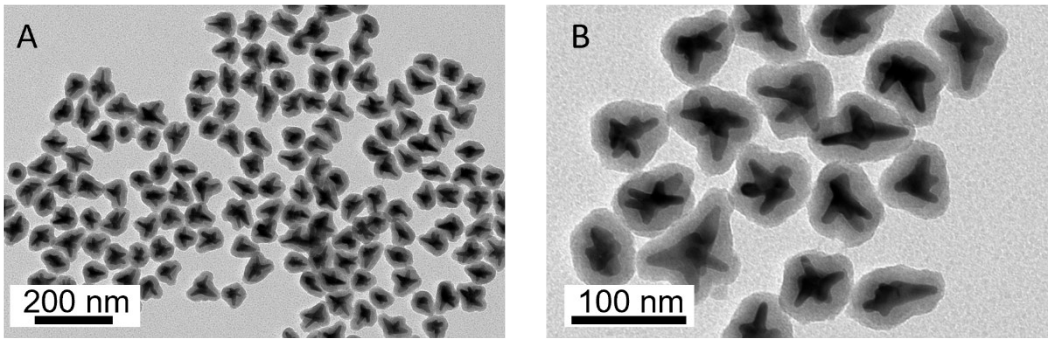

Figure S20. Representative TEM images of silica-coated nanoparticles with plasmon band centered at 900 nm.

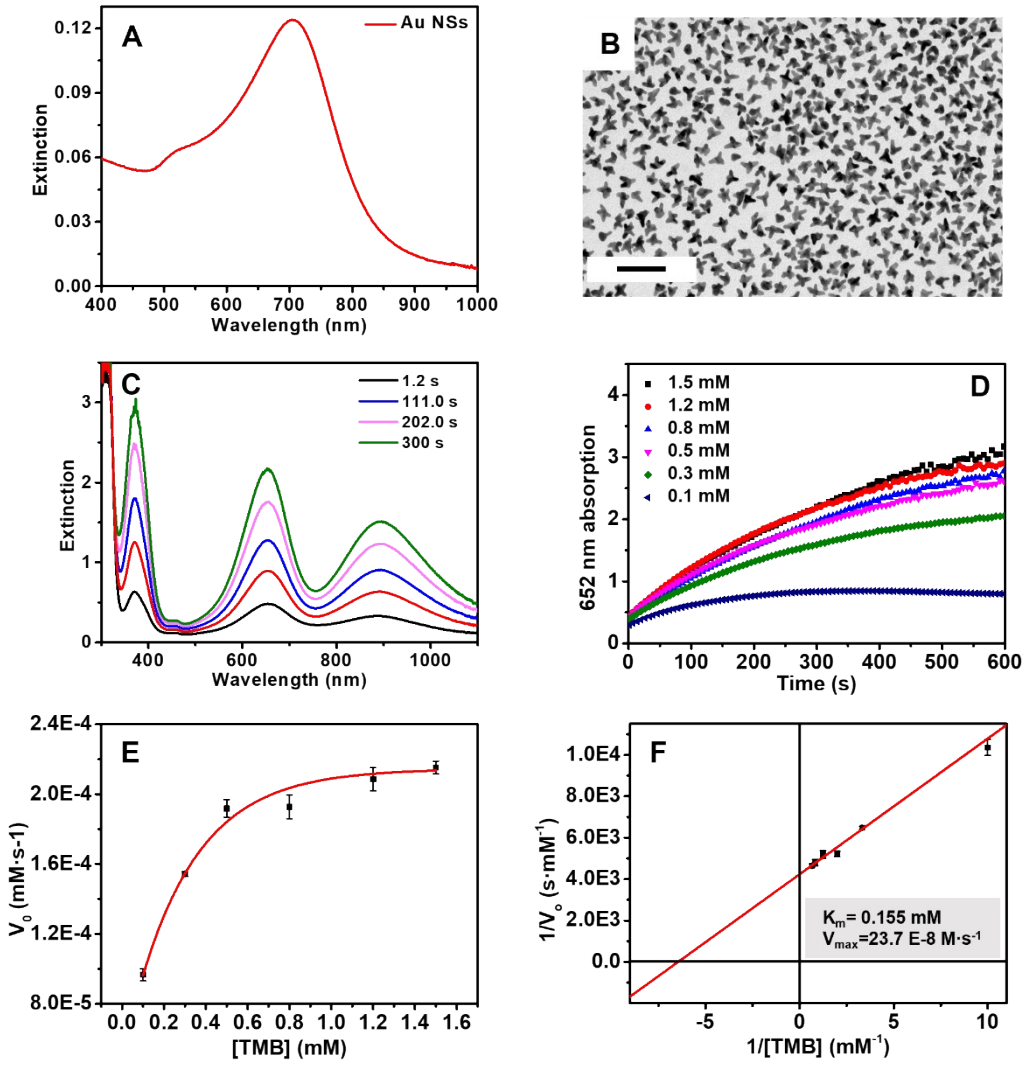

Figure S21. Results of AuNS700 as the catalyst, varying TMB. (A) Vis-NIR extinction spectra and (B) TEM image of the AuNSs used as catalysts. The scale bar is 100 nm (C) Time evolution absorption spectra of the oxidation of TMB. (D) Time evolution of the absorbance at 652 nm for different concentrations of TMB substrate, as indicated. (E) Michaelis-Menten curve of AuNSs nanozymes. (F) The double reciprocal plots of TMB obtained from the Michaelis-Menten curve. Error bars represent the standard deviation derived from three independent experiments.

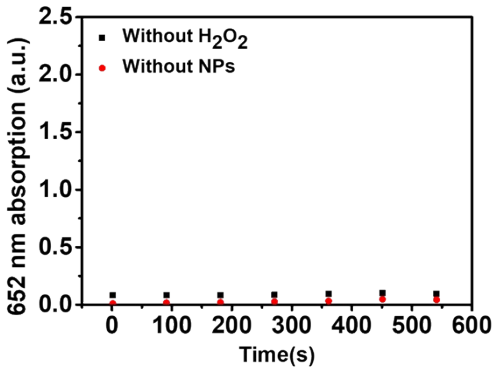

Figure S22. Time-dependent change in absorbance of oxidized TMB at 652 nm in the absence of AuNSs or hydrogen peroxide.

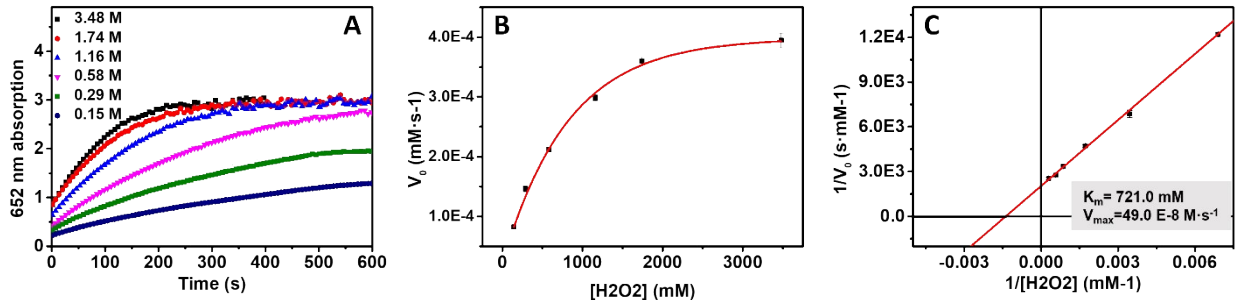

Figure S23. Results of $AuNS_{700}$ as the catalyst, varying H_2O_2. (A) Time evolution of the absorbance at 652 nm for different concentrations of H_2O_2, as indicated. (B) Michaelis-Menten curve of AuNSs nanozymes. (C) The double reciprocal plots of H_2O_2 obtained from the Michaelis-Menten Curve. Error bars represent standard deviation derived from three independent experiments.

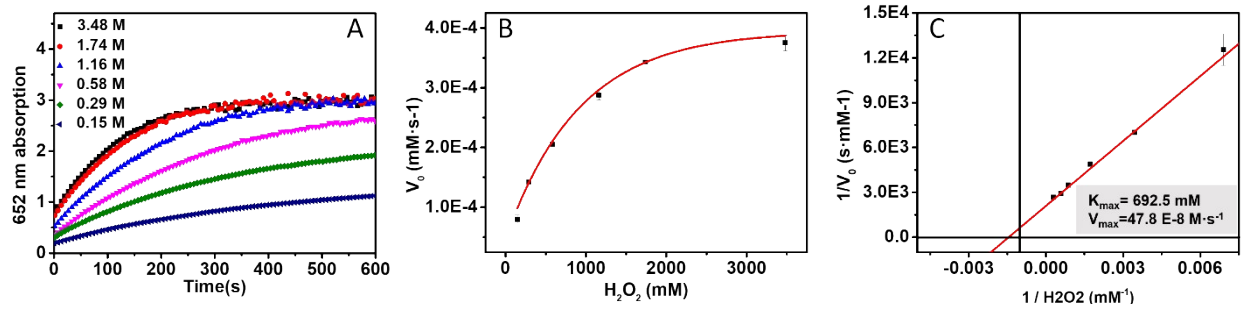

Figure S24. Results of $AuNS_{850}$ as the catalyst, varying H_2O_2. (A) Time evolution of the absorbance at 652 nm for different concentrations of H_2O_2, as indicated. (B) Michaelis-Menten curve of AuNSs nanozymes. (C) The double reciprocal plots of H_2O_2 obtained from the Michaelis-Menten curve. Error bars represent standard deviation derived from three independent experiments.

Table S1. Summary of different synthesis protocols of gold nanostars and their properties.

Growth strategy	Seeds*	Reductor/Stabilizing molecules	Shape directors	Overall Dimension range/Yield	Main LSPR (nm)	Long-term stability	Ref.
Seeded	Au, 15nm	DMF/PVP	PVP and seed crystal structure	~70nm/~100%	Broad, 764	Stable long time at RT	3
Seeded	Au, 15nm	DMF/PVP	PVP and seed crystal structure	~45-116nm/ ~100%	Broad, 700-850	Stable long time at RT	4
Seeded	Pt, 2.5nm	DMF/PVP	PVP and seed crystal structure	~9-30nm/~100%	Narrow, 550-750	Stable long time at RT	5
Seeded	Au, 30 nm	DMF/PVP	PVP and seed crystal structure	~34-60 nm/~100%	Narrow, 550-880	Stable long time at RT	6
Seeded	Au, 5 nm	AA/PAH	PAH and seed crystal structure	~70-150nm/~100%	Broad, 580-1250	Stable long time at RT	7
Seedless	-	Fe(II)/PSS	PSS	~70-15 nm/~100%	Broad, 580-750	Stable long time at RT	8
Seeded	Ag, 15nm	AA/CTAB	CTAB and NaOH	~50nm/45%	670	Stable <20 days a RT	9
Seedless	-	AA/Triton X	Triton X as LLC template	n.d./n.d.	Broad, 550-650	Unstable	10
Seeded	Au, 2.5nm	AA/SDS	SDS and seed crystal structure	~40nm/n.d.	Broad, 550-612	Unstable	11
Seedless	-	AA/AOT-BDAC	AOT-BDAC and Ag^+	~74-196 nm/n.d.	Broad, 670-1000	Unstable	12
Seeded	Au, <4nm	AA/LBL	LBL and Ag^+	~55-100nm/~90%	Broad, 700-1100	Unstable	13
Seeded	Au, 2-3nm	AA/CTAB	CTAB and Ag^+	~174nm/70%	n.d.	n.d.	14
Seeded	Au, n.d.	AA/Triton X	Triton X and Ag^+	n.d./n.d.	Narrow, 600-1600	Unstable	15
Seedless	-	AA/Triton X	Triton X and Ag^+	~50-300nm/~100%	Broad, 700-2000	Unstable	16
Seedless	-	NH_2OH/Ag^+	NH_2OH/Ag^+	~100-300 nm/n.d.	Broad, 600-1100	n.d.	17
Seeded	Au, 5 or 12 nm	AA/ Ag^+	Ag^+ and seed crystal structure	~60-190 nm/100%	Broad, 650-800	Stable at 4◦C	18
Seeded		HQ/SC	HQ/SC and seed crystal structure	~55-200 nm/100%	Narrow, 555-702	Stable <10 days	19

						a RT	
Seedless	-	H_2O_2/SC-BSPP	BSPP and seed crystal structure	~45 nm/90%	Narrow, 650-700	Stable	20
Seedless	-	Good´s Buffers	Goods Buffers	20-70nm/n.d.	Broad, 550-650	Stable at 4◦C	21
Seedless	-	AA/ HEPES	HEPES	~30-50nm/92%	Broad, 550-700	Stable at 4◦C	22
Seedless	-	AA/ Good Buffers	Good buffers	50 nm/95%	Broad, 600-1100	Stable at 4◦C	23
Seeded	Au, 40 or 60 nm	NH_2OH/HEPES	HEPES/SC	50-100nm/100%	Narrow, 550-750	Stable	24
Seeded	Au, 30, 60 or 100 nm	AA/Goods Buffers	Goods Buffers	40-150nm/100%	Narrow, 650-1000	n.d.	25
Seedless	-	AA/BSA	BSA and seed crystal structure	~96-100/n.d.	Broad ~760	Stable long time at RT	26
Seeded	Ag, 4nm	AA/Gelatin	Gelatin and seed crystal structure	45nm/90%	Narrow, 550-650	Stable	27
Seedless	-	L-Dopa	L-Dopa	30-60nm/100%	Broad, 600-850	Stable	28
Seedless	-	Trp-GA	Trp-GA	200-1000nm/n.d.	Broad, 750	Stable	29
Seedles	-	L-AA/5'-GMP	L-AA/5'-GMP	~65nm/~100%	Broad, 650	Stable	30

n.d. (Not determined)
* **Composition/Size**

Table S2. Comparing the kinetic parameters (K_m and V_{max}) of the nanostars of the present work with other reported metallic nanomaterials. K_m is the Michaelis-Menten constant, and V_{max} is the maximum reaction velocity.

Catalyst	K_m (mM)		V_{max} (10^{-8} M·s^{-1})		Ref
	TMB	H_2O_2	TMB	H_2O_2	
850 nm NanoStars@AMP	0.154	692.5	23.5	47.8	This work
700 nm NanoStars@AMP	0.155	721	23.7	49.0	This work
HRP	0.434	3.70	10.0	8.71	31
TA – capped AuNPs	0.2	190	6.7	3.8	32
BSA-Au	0.00253	25.3	6.23	7.21	33
Citrate AuNPs	0.134	213	9.65	10.6	34
Citrate AuNPs + ATP	0.168	196	13.1	9.83	34
PEG AuNPs	0.155	191	8.32	6.38	34
Au-Ag CSPNPs	0.369	94.7	1.41	2.92	35
Pt NCs	0.096	3.07	14.1	18.17	36
Au-$PtNCs_2$	0.108	-	106	-	37

References

1 P. Gruszczyński, K. Smalara, M. Obuchowski and R. Kaźmierkiewicz, *J. Mol. Model.*, 2011, **17**, 1081–1090.
2 E. Kobayashi, K. Yura and Y. Nagai, *Biophysics (Oxf).*, 2013, **9**, 1–12.
3 P. Senthil Kumar, I. Pastoriza-Santos, B. Rodríguez-González, F. Javier García de Abajo and L. M. Liz-Marzán, *Nanotechnology*, 2008, **19**, 015606.
4 C. G. Khoury and T. Vo-Dinh, *J. Phys. Chem. C*, 2008, **112**, 18849–18859.
5 S. Barbosa, A. Agrawal, L. Rodríguez-Lorenzo, I. Pastoriza-Santos, R. A. Alvarez-Puebla, A. Kornowski, H. Weller and L. M. Liz-Marzán, *Langmuir*, 2010, **26**, 14943–14950.
6 D. Y. Kim, T. Yu, E. C. Cho, Y. Ma, O. O. Park and Y. Xia, *Angew. Chemie - Int. Ed.*, 2011, **50**, 6328–6331.
7 S. Nuti, C. Fernández-Lodeiro, J. Fernández-Lodeiro, A. Fernández-Lodeiro, J. Pérez-Juste, I. Pastoriza-Santos, A. P. LaGrow, O. Schraidt, J. Luis Capelo-Martínez and C. Lodeiro, *J. Colloid Interface Sci.*, 2022, **611**, 695–705.
8 J. Djafari, A. Fernández-Lodeiro, D. García-Lojo, J. Fernández-Lodeiro, B. Rodríguez-González, I. Pastoriza-Santos, J. Pérez-Juste, J. L. Capelo and C. Lodeiro, *ACS Sustain. Chem. Eng.*, 2019, **7**, 8295–8302.
9 S. Chen, Z. L. Wang, J. Ballato, S. H. Foulger and D. L. Carroll, *J. Am. Chem. Soc.*, 2003, **125**, 16186–16187.
10 S. Umadevi, H. C. Lee, V. Ganesh, X. Feng and T. Hegmann, *Liq. Cryst.*, 2014, **41**, 265–276.
11 C. H. Kuo and M. H. Huang, *Langmuir*, 2005, **21**, 2012–2016.
12 F. Liebig, R. Henning, R. M. Sarhan, C. Prietzel, C. N. Z. Schmitt, M. Bargheer and J. Koetz, *RSC Adv.*, 2019, **9**, 23633–23641.
13 P. Pallavicini, G. Chirico, M. Collini, G. Dacarro, A. Donà, L. D'Alfonso, A. Falqui, Y. Diaz-Fernandez, S. Freddi, B. Garofalo, A. Genovese, L. Sironi and A. Taglietti, *Chem. Commun.*, 2011, **47**, 1315–1317.
14 T. K. Sau and C. J. Murphy, *J. Am. Chem. Soc.*, 2004, **126**, 8648–8649.
15 P. Pallavicini, A. Donà, A. Casu, G. Chirico, M. Collini, G. Dacarro, A. Falqui, C. Milanese, L. Sironi and A. Taglietti, *Chem. Commun.*, 2013, **49**, 6265–6267.
16 A. J. Blanch, M. Döblinger and J. Rodríguez-Fernández, *Small*, 2015, **11**, 4549–4549.
17 H. Yuan, W. Ma, C. Chen, J. Zhao, J. Liu, H. Zhu and X. Gao, *Chem. Mater.*, 2007, **19**, 1592–1600.
18 H. Yuan, C. G. Khoury, H. Hwang, C. M. Wilson, G. A. Grant and T. Vo-Dinh, *Nanotechnology*, 2012, **23**, 075102.
19 J. Li, J. Wu, X. Zhang, Y. Liu, D. Zhou, H. Sun, H. Zhang and B. Yang, *J. Phys. Chem. C*, 2011, **115**, 3630–3637.
20 E. Hao, R. C. Bailey, G. C. Schatz, J. T. Hupp and S. Li, *Nano Lett.*, 2004, **4**, 327–330.
21 A. Habib, M. Tabata and Y. G. Wu, *Bull. Chem. Soc. Jpn.*, 2005, **78**, 262–269.
22 J. Xie, J. Y. Lee and D. I. C. Wang, *Chem. Mater.*, 2007, **19**, 2823–2830.
23 K. Chandra, K. S. B. Culver, S. E. Werner, R. C. Lee and T. W. Odom, *Chem. Mater.*, 2016, **28**, 6763–6769.
24 G. Maiorano, L. Rizzello, M. A. Malvindi, S. S. Shankar, L. Martiradonna, A. Falqui, R. Cingolani and P. P. Pompa, *Nanoscale*, 2011, **3**, 2227–2232.
25 R. M. Pallares, T. Stilson, P. Choo, J. Hu and T. W. Odom, *ACS Appl. Nano Mater.*,

2019, **2**, 5266–5271.
26 J. Li, R. Cai, N. Kawazoe and G. Chen, *J. Mater. Chem. B*, 2015, **3**, 5806–5814.
27 L. Lu, K. Ai and Y. Ozaki, *Langmuir*, 2008, **24**, 1058–1063.
28 M. Sajitha, A. Vindhyasarumi, A. Gopi and K. Yoosaf, *RSC Adv.*, 2015, **5**, 98318–98324.
29 P. Bian, J. Yuan, H. Han and Z. Ma, *J. Nanosci. Nanotechnol.*, 2016, **16**, 7503–7508.
30 P. Huang, O. Pandoli, X. Wang, Z. Wang, Z. Li, C. Zhang, F. Chen, J. Lin, D. Cui and X. Chen, *Nano Res.*, 2012, **5**, 630–639.
31 L. Gao, J. Zhuang, L. Nie, J. Zhang, Y. Zhang, N. Gu, T. Wang, J. Feng, D. Yang, S. Perrett and X. Yan, *Nat. Nanotechnol.*, 2007, **2**, 577–583.
32 K. V. Serebrennikova, N. S. Komova, A. N. Berlina, A. V. Zherdev and B. B. Dzantiev, *Chemosensors*, 2021, **9**, 332.
33 X.-X. Wang, Q. Wu, Z. Shan and Q.-M. Huang, *Biosens. Bioelectron.*, 2011, **26**, 3614–3619.
34 J. Shah and S. Singh, *3 Biotech*, 2018, **8**, 67.
35 J. Li, G. Zhang, L. Wang, A. Shen and J. Hu, *Talanta*, 2015, **140**, 204–211.
36 L. Jin, Z. Meng, Y. Zhang, S. Cai, Z. Zhang, C. Li, L. Shang and Y. Shen, *ACS Appl. Mater. Interfaces*, 2017, **9**, 10027–10033.
37 Y.-C. Gao, C. Wang, C.-X. Zhang, H.-W. Li and Y. Wu, *J. Mater. Sci. Technol.*, 2022, **109**, 140–146.